U. Ilangovan
A. Ramamoorthy
Biophysics Research Division and Department of Chemistry, The University of Michigan, Ann Arbor, MI 48109-1055, USA

Received 24 April 1997; accepted 6 August 1997

Conformational Studies of Human Islet Amyloid Peptide Using Molecular Dynamics and Simulated Annealing Methods

Abstract: *Molecular dynamics simulations and simulated annealing in vacuum, model aqueous solution, and simulated membrane were used to analyze the conformational preferences of a segment spanning 20–29 residues of human islet amyloid polypeptide,* [*referred to as* $IAPP^H(20–29)$]. *Molecular dynamics simulations were conducted at 300 K on* $IAPP^H(20–29)$. *The minimum energy conformers obtained in model aqueous solution and vacuum exhibited similar structures. Even in the absence of any constraints on peptide bonds,* trans *conformation was preferred consistently by all the peptide bonds. Analysis of the minimum energy conformers indicated that* $IAPP^H(20–29)$ *showed a strong preference for* turn *structures in all the environments. These turn structures were stabilized by the formation of hydrogen bonds between the backbone amide and carbonyl groups. A good agreement was found between the results obtained from the molecular dynamics simulation and solid-state nmr experimental studies.* © *1998 John Wiley & Sons, Inc. Biopoly* ***45:*** *9–20, 1998*

Keywords: *islet amyloid peptide; amylin peptide; human amylin; molecular dynamics; simulated annealing; conformation*

INTRODUCTION

Amylin, a 37 amino acid residue polypeptide hormone,[1] is the principal constituent of the amyloid deposits that form in the islets of Langerhans in the pancreases of patients with type II diabetes mellitus or noninsulin-dependent diabetes mellitus (NIDDM).[2–6] Interest in this peptide stems from its pivotal role as an important regulatory hormone inhibiting basal and insulin-stimulated glucose uptake as well as glycogen synthesis in muscle.[2–7] The amount of amylin deposited is proportional to the insulin requirements of the patient and thus to the clinical severity of the disease. It has been shown in vitro that amyloidogenic human amylin is more toxic to insulin-producing β-cells than nonamyloidogenic rat amylin.[7] Human amylin forms amyloid fibrils and its interaction with cell membranes is necessary for toxicity. Recent studies predict that human amylin at cytotoxic concentrations forms voltage-dependent, relatively nonselective, ion-permeable channels in phospholipid bilayer membranes, whereas rat amylin does not form channels.[8] The relatively poor selectivity of human amylin channels would tend to lead to disruptions of ionic homeostasis, including influxes of Ca^{2+} and Na^+, and effluxes of K^+ and other vital cellular constituents. Prolonged elevations of intracellular Ca^{2+} levels, for example, may lead to cellular damage and even death. Thus increased hu-

Correspondence to: A. Ramamoorthy
Contract grant sponsor: Biophysics Research Division and Department of Chemistry
Biopolymers, Vol. 45, 9–20 (1998)

CCC 0006-3525/98/010009-12

man amylin deposition may lead to increased channel formation and β-cell destruction, thereby increasing the insulin requirement.

The primary amino acid sequences of human and rat amyloid polypeptides are given below. Underlined residues represent the nonconservative differences in the sequences. Although the primary amino acid sequence of human and rat amylin exhibit 84% sequence homology, their effects on the organism differ dramatically, which is attributed to secondary structural differences between them. The segment (20–29) is thought to be responsible for human amylin's ability to insert into the β-cell membrane and form active ion channels in the phospholipid bilayer. Studies have shown that mutation at any one of these sites abolishes the capacity of human amylin to form ion-permeable pores.

```
                1                   10
Human amylin    K C N T A T C A T Q R L A N F
Rat amylin      K C N T A T C A T Q R L A N F

                    20                  30          37
                L V H S S N N F G A I L S S T N V G S N T Y
                L V R S S N N L G P V L P P T N V G S N T Y
```

The fact that rat amylin, unlike human amylin, does not form amyloid fibrils in vitro or in vivo, does not form ion-permeable channels, and is less toxic suggests a strong relationship between the structure and toxicity.[7–16] In spite of the evident relationship between the structure and toxicity, a complete study on the structure and function of amylin peptides is clearly lacking. A detailed structural analysis of the amylin peptide, both in solution and when interacting with the lipid bilayers, will be useful to design molecules that will bind to amylin attempting to reduce its deleterious effects on patients with NIDDM.

Results from x-ray crystallographic studies reveal a β-pleated sheet structure in a synthetic peptide corresponding to residues 20–29 of human amylin.[1] Experimental studies on the synthetic amylin peptides using CD[15] and NMR spectroscopy suggest that human amylin interacts with phosphatidylcholine membranes and adopts a β-sheet structure, while in trifluoroethanol (TFE) the structure is primarily α-helical.[15,16] This β-sheet structure is dramatically different from that of amphipathic α-helical peptides whose structure is α-helical both in TFE and 1,2-dimyristoyl-3-phosphatidylcholine. This could be due to the promotion of peptide–peptide interactions in a lipid environment and with less interaction in the aqueous phase. On the other hand, in TFE, the peptide may exist in a monomeric state where it adopts an α-helical structure. Fourier transform ir (FTIR) spectroscopy of human islet amyloid polypeptide [$IAPP^H(20–29)$] suggests that the peptide forms amyloid fibril containing antiparallel β-sheet structure.[17] The secondary structure of a 10-residue synthetic peptide based on residues 20–29 of amylin, in powder form, has recently been studied using the rotational resonance solid-state nmr method.[10] In this study, six intramolecular-intercarbon distances were used to determine the highly pleated β-sheet structure. The toxic effect of fibrillar amylin is strikingly similar to that of the β-amyloid protein[9] *and* of a peptide from the prion protein,[7] which forms amyloid fibrils in Alzheimer's disease[14] and the spongiform encephalopathies,[13] respectively.

Due to the noncrystalline nature and low solubility under physiological condition of the amyloid fibrils, human amylin is not amenable for traditional structural studies using x-ray crystallography and multidimensional solution nmr methods. Only the solid-state nmr (SSNMR) technique has been used to provide some structural details.[10] Studies using CD and solution-state nmr experiments failed to provide atomic-level details of the structure.[15,16] On the other hand, even though the structure of 10-residue peptide determined through rotational resonance SSNMR method is of high accuracy,[10] the very important information about the interaction of amylin with membranes is not known. Even though the detailed structural information obtained from experimental studies is thus far inconclusive, this information when used in conjunction with modern computational techniques can greatly facilitate the elucidation of a reasonable or accurate three-dimensional structure of human amylin peptide.

Molecular dynamics (MD) methods have been shown to be extremely powerful in finding structural models of polypeptides in membrane and solutions after exploring various conformational spaces accessible to the peptide. Usually, experimental data obtained through nmr spectroscopy are used in combination with computational techniques such as distance geometry,[18,19] molecular dynamics,[20–25] simulated annealing,[26] and variable target algorithm[27] to yield the desired three-dimensional structure. The main objective of this study is to search the conformational space of the peptide fragment (residues 20–29) of human amylin in various environments. A detailed analysis of the conformation of amylin peptide in vacuum, model aqueous solution, and simulated membrane environments using MD simulations and simulated annealing is presented. Molec-

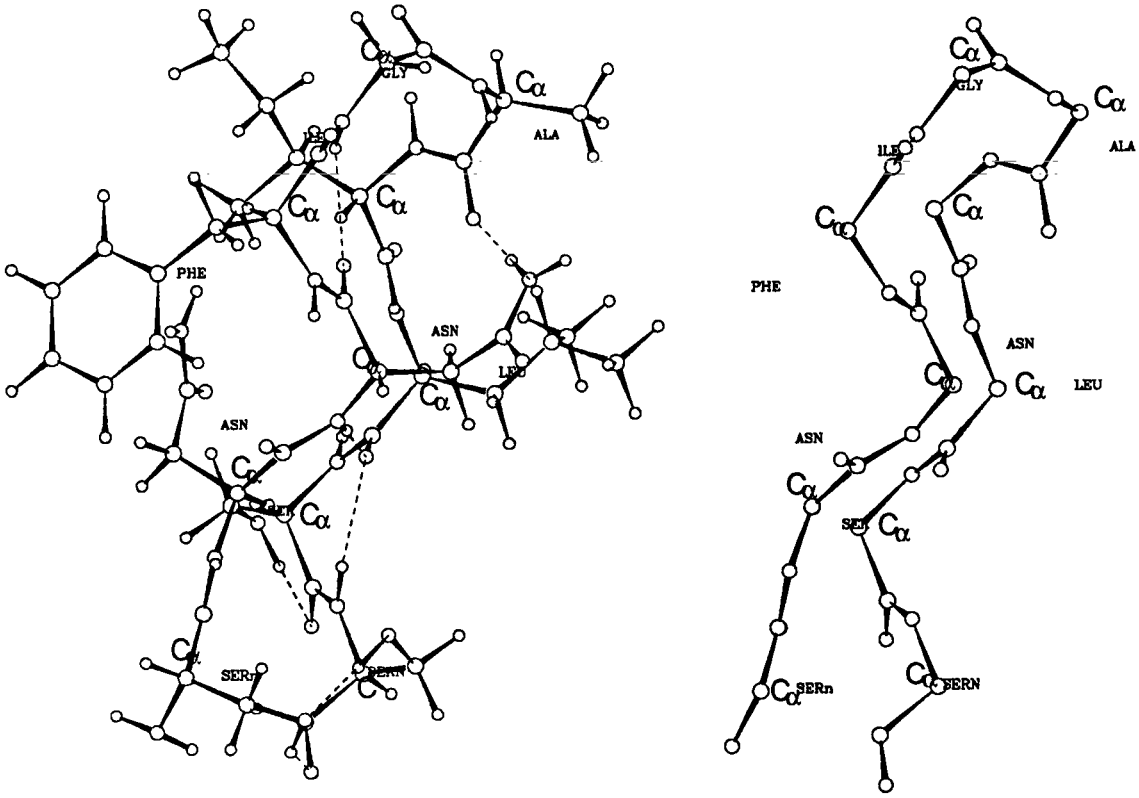

FIGURE 1 Minimum energy structure obtained in the 20 ps unrestrained molecular dynamics analysis of IAPP^{H}(20–29) in vacuum. Conformational parameters for this structure are given in Table I and Table IV. Hydrogen atoms of the peptide are not shown. The dotted lines indicate hydrogen bonding. Backbone conformation is shown on the right side for clarity.

ular dynamics results are compared with the structural informations obtained through SSNMR experiments.

FIGURE 2 Superposition of backbone atoms of the low energy structures of IAPP^{H}(20–29) found along the trajectory of 20 ps molecular dynamics simulations under vacuum.

METHODS

MD simulations and other computational procedures were performed with DISCOVER and INSIGHT (Biosym Inc., San Diego, USA) packages on Silicon Graphics RS5000 Workstations. Starting configuration for all the peptides were generated using INSIGHT. The starting configuration was linear, corresponding to an all-*trans* backbone configuration. The fully extended conformations (ϕ, ψ, $\omega = 180°$) were subjected to energy minimization in order to generate starting structures for MD. No Morse potentials or cross terms were used. Energy minimization carried out consisted of few steps of steepest descents followed by the conjugate gradient method. Structures were minimized until the maximum derivative was less than 0.001 kcal/(mol-Å). The model membrane environment of the peptide was simulated by setting the dielectric constant to 2.0. The solvent water was modeled using a dielectric constant, $\varepsilon = 80$. Although it is recognized that these values provide only a macroscopic representation of dielectric effects, their use may be justified under certain circumstances.[28] The consistent valence force field was used in all the potential energy calculations.

Unrestrained room temperature molecular dynamics

Table I Dihedral Angles of the Minimum Energy Conformation of IAPP^{H} (20–29) in Vacuum Obtained Using Molecular Dynamics Simulations

Residue	ϕ	ψ	ω	1χ	2χ	3χ	4χ
Ser20		165.3	174.9	70.7			
Asn21	−149.0	139.4	170.0	−173.5	75.0		
Asn22	−81.0	107.6	−172.9	−166.5	69.0		
Phe23	−87.0	90.2	−177.9	−73.1	96.3	−179.3	−0.2
Gly24	162.2	−82.8	155.1				
Ala25	−82.0	105.2	−160.0				
Ile26	−76.1	101.7	−179.4	−61.5	162.1		
Leu27	−125.8	114.0	−175.2	−63.4	171.7		
Ser28	−83.4	81.3	176.8	68.4			
Ser29	−81.8			57.5			

simulations of IAPP^{H}(20–29) were carried out in vacuum, dielectric 2, and dielectric 80 environments. Energy-minimized structures were equilibrated by running dynamics at 300 K for 2000 iterations with a step of 1 fs. Data were collected from a subsequent 20 ps dynamics run. By this procedure a total of 20,000 configurations (one every 10^{-15} s) were sampled during MD for each system. To reduce the volume of data to a more manageable level, the instantaneous configurations selected at 1 ps intervals along molecular dynamics trajectories were minimized, allowing all atoms to move with 100 steps of steepest descent and the conjugate gradient method until the maximum derivative was smaller than 0.001 kcal/(mol-Å). Normally, the minimization process took between 3000–5000 iterations and led to average derivatives around 0.00018 kcal/(mol-Å).

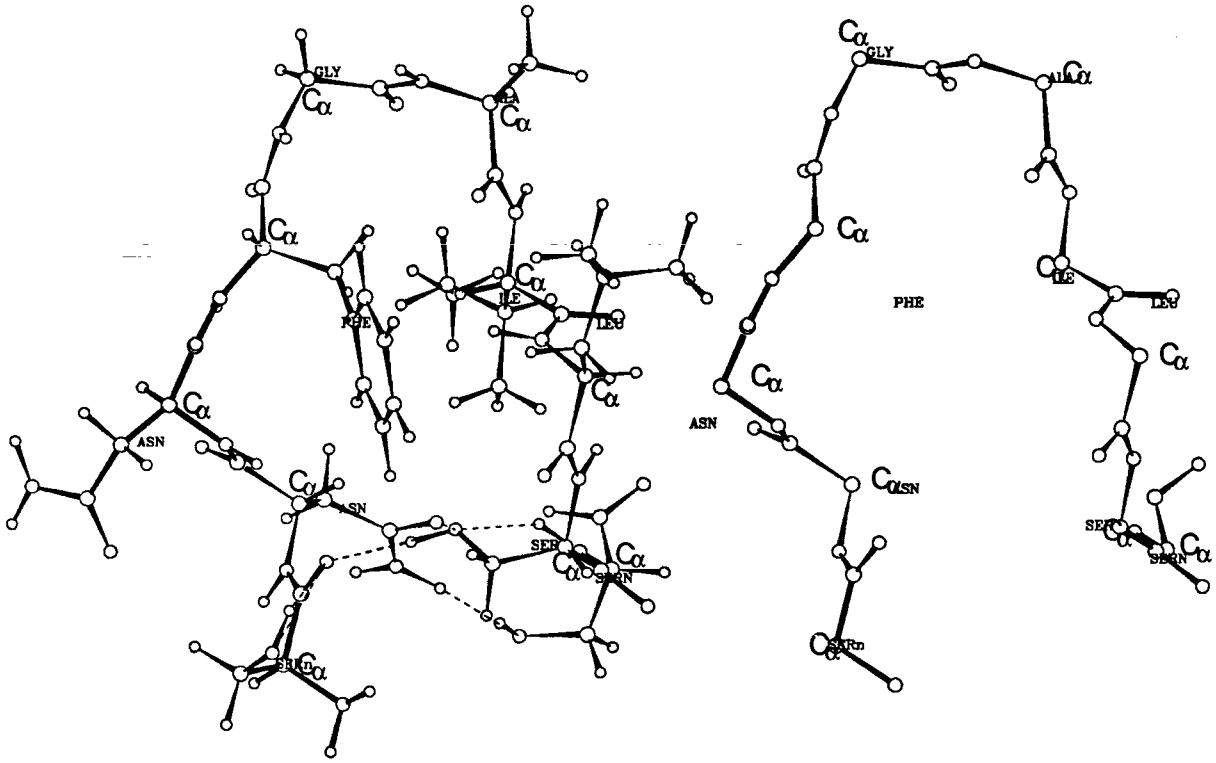

FIGURE 3 Minimum energy structure obtained in the 20 ps unrestrained molecular dynamics analysis of IAPP^{H}(20–29) in membrane. Conformational parameters for this structure are given in Table II and Table IV. Hydrogen atoms of the peptide are not shown. The dotted lines indicate hydrogen bonding. Backbone conformation is shown on the right side for clarity.

FIGURE 4 Superposition of backbone atoms of the low energy structures of IAPP^{H}(20–29) found along the trajectory of 20 ps molecular dynamics simulations under membrane.

RESULTS AND DISCUSSION

Unrestrained MD of IAPP^{H}(20–29)

The energy of a fully extended starting configuration of IAPP^{H}(20–29) was 168.24 kcal/mol. Initial energy minimization was carried out using the steepest descents method for 100 iterations. Further minimization was carried out by conjugate gradient method until the maximum derivative was smaller than 0.001 kcal/(mol-Å). This two-step minimization procedure yielded the initial conformation of the IAPP^{H}(20–29), which is suitable for MD simulation studies with an energy of 99.59 kcal/mol. Room temperature molecular dynamics simulations on this initial conformation were carried out for 20 ps at 300 K. The minimum energy conformation found along the trajectory had an energy of 78.69 kcal/mol and is shown in Figure 1.

MD simulation yielded 21 structures in accordance with the method described in the previous section. Analysis of the trajectory of MD simulations carried out on IAPP^{H}(20–29) in vacuum revealed the existence of two types of families of conformers. Out of these two, only one possessed predominantly *turn* structures. Similar structural features were not observed in the other type of family. Interestingly, the family comprising conformers of turn structures mainly adapted consistently low energy conformations. The average energy of all these structures was calculated to be 79.22 kcal/mol. These structures are shown in Figure 2 with only backbone atoms of residues superimposed onto each other. The rms deviations for these structures range from 0.4 to 2.5 Å. Figure 2 also illustrates how the initial conformation of IAPP^{H}(20–29) converged to turn structures during these 20 ps MD simulation carried out under vacuum.

The dihedral angles (ϕ,ψ) measured from the minimum energy conformer, shown in Figure 1, are summarized in Table I. As it is evident from the ω values in Table I, the peptide bonds have not undergone any *trans–cis* isomerism even in the absence of any torsional constraints imposed on the peptide bonds. Examination of the dihedral angles presented in Table I reveals that, except Gly24, all other residues assume negative ϕ values and positive ψ values. This observation indicates that the position of Gly residue in IAPP^{H}(20–29) plays an important role in the formation of turn structures. In this conformation, Gly24 and Ala25 residues form the central residues of a β-turn like structure. The minimum energy structure shows that there are 7 hydrogen bonds possible in this conformation.

Table II Dihedral Angles of the Minimum Energy Conformation of IAPP^{H} (20–29) in a Model Membrane Environment Obtained Using Molecular Dynamics Simulations

Residue	ϕ	ψ	ω	1χ	2χ	3χ	4χ
Ser20		110.0	178.9	62.6			
Asn21	−95.5	79.3	180.0	−65.5	−45.7		
Asn22	−125.0	78.4	−161.4	−66.9	90.6		
Phe23	−157.3	156.2	153.4	−76.8	106.6	177.9	−1.0
Gly24	−78.4	−74.7	166.1				
Ala25	−83.1	116.2	−164.6				
Ile26	−80.2	109.9	174.1	−60.2	162.8		
Leu27	−108.2	67.5	179.9	−62.8	172.3		
Ser28	−164.2	−71.1	177.7	57.3			
Ser29	−151.4			58.7			

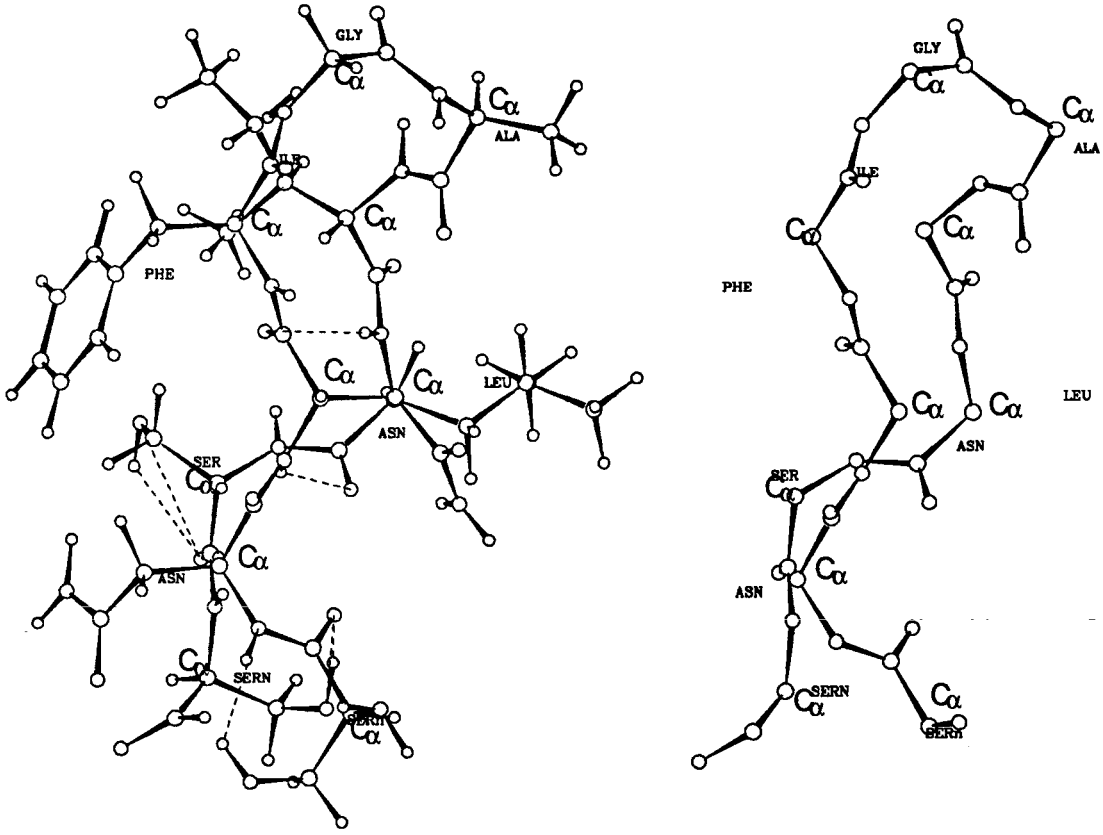

FIGURE 5 Minimum energy structure obtained in the 20 ps unrestrained molecular dynamics analysis of $IAPP^H(20-29)$ in a model aqueous solution. Conformational parameters for this structure are given in Table III and Table IV. Hydrogen atoms of the peptide are not shown. The dotted lines indicate hydrogen bonding. Backbone conformation is shown on the right side for clarity.

Also, hydrogen bonding between Gly24 NH and Asn22 CO and Ser29 NH and Leu27 CO indicates the formation of γ-turns around Phe23 and Ser28, respectively. In addition to this, there is also hydrogen bonding between Asn22 NH and Leu27 CO. The hydrogen bonding data obtained from the minimum energy conformations are summarized in Table IV.

To perform MD simulations on $IAPP^H(20-29)$ in a model membrane environment, the dielectric constant ε was set to 2.0, as it has been shown to faithfully mimic the membrane environment for peptides and proteins.[29] The structure resulting after the initial two-step energy minimization with an energy of 99.59 kcal/mol was subjected to 20 ps of unrestrained MD simulations at 300 K. The minimum energy conformation visited along the trajectory, shown in Figure 3, had an energy of 101.7 kcal/mol. In the membrane environment also, $IAPP^H(20-29)$ forms a turn structure around residues 24 and 25. However, the results obtained from the MD simulations of $IAPP^H(20-29)$ in the model membrane environment are different from those obtained in vacuum in two respects: (a) in the model membrane environment, the sterically hindering bulky phenyl ring of Phe23 moves into close proximity with the side-chain atoms of Ile26 as evident from Figure 3; and (b) the structures in the model membrane do not have most of the hydrogen bonds that were present in the vacuum structure as evident from the data given in Table IV. The energy of the average conformation of all these structures in the model membrane is 108.18 kcal/mol. The rms deviations for these structures range from 0.5 to 3.0 Å. Figure 4 presents the superimposition of backbone atoms of the structures obtained from the MD trajectories.

The dihedral angles obtained from the minimum energy structure, shown in Figure 3, are given in Table II. It is clear from the ω values that the peptide

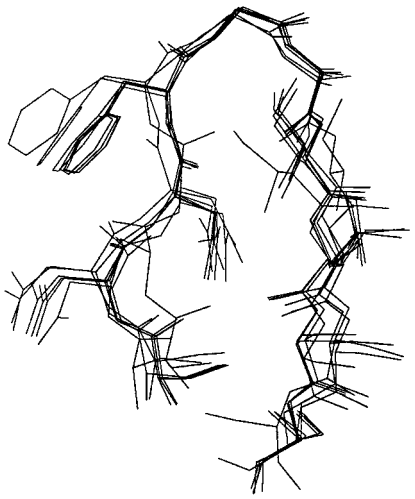

FIGURE 6 Superposition of backbone atoms of the low energy structures of IAPP^{H}(20–29) found along the trajectory of 20 ps molecular dynamics simulations under a model aqueous solution.

bonds of IAPP^{H}(20–29) have not undergone any drastic change in the presence of membrane environment. All the residues of IAPP^{H}(20–29) assume ϕ values ranging from $-80°$ to $-165°$. A careful examination of ϕ,ψ values of Gly24 and Ala25 residues may indicate a type VIII β-turn,[30] although the ϕ,ψ values vary from the ideal β-turn by $\pm 30°$.

To study the effect of solvent on conformational behavior of IAPP^{H}(20–29), MD simulations were carried out under model aqueous solution environment after modeling the solvent system as described in the previous section. The minimum energy conformation obtained in model aqueous solution is shown in Figure 5. It is obvious that, in the model aqueous solution environment also, IAPP^{H}(20–29) shows a strong preference to form a turn structure only around Gly24 and Ala25 residues. The overall secondary structures of the peptide in model aqueous solution and vacuum are similar. However, the energy of the minimum energy conformation in model aqueous solution is 94.18 kcal/mol, which is 17.48 kcal/mol more than the value obtained in vacuum. Further analysis of the MD trajectory of IAPP^{H}(20–29) in model aqueous solution reveals that the peptide bonds always remain in the *trans* conformation. Even in the absence of any constraint on peptide bonds, the ω values vary from $-158°$ to 151°. Figure 6 presents the superimposition of backbone atoms of the structures obtained from the MD trajectories. The dihedral angles (ϕ,ψ) measured from the minimum energy conformer, shown in Figure 5, are summarized in Table III for the model aqueous solution environment.

Hydrogen Bonds

Various types of hydrogen bonds that are summarized in Table IV stabilize turn structures observed in IAPP^{H}(20–29). The hydrogen bonds formed between atoms of the same residue and that of adjacent residues are not given. The minimum energy conformation of IAPP^{H}(20–29) peptide in vacuum is stabilized by 7 hydrogen bonds. On the other hand, the minimum energy conformation in model membrane and model aqueous solution are stabilized by 4 and 6 hydrogen bonds, respectively. Hydrogen bonding between Asn22 NH and Leu27 CO was found both in vacuum and model aqueous solution environments. A significant observation was noticed in the MD analysis of IAPP^{H}(20–29) in dielectric 80 is the presence of *trans* annular hydrogen bonds between Asn22 NH and Leu27 CO and Asn22 CO

Table III Dihedral Angles of the Minimum Energy Conformation of IAPP^{H} (20–29) in a Model Aqueous Solution Environment Obtained Using Molecular Dynamics Simulations

Residue	ϕ	ψ	ω	1χ	2χ	3χ	4χ
Ser20		−62.2	179.2	65.1			
Asn21	−85.8	110.0	−179.0	−73.2	87.8		
Asn22	−116.9	133.7	−178.1	−67.2	−72.9		
Phe23	−140.7	131.0	−164.2	−71.1	100.9	−178.4	−0.1
Gly24	124.4	−85.0	151.8				
Ala25	−87.8	103.3	−158.4				
Ile26	−87.0	107.9	166.3	−56.2	165.8		
Leu27	−130.6	83.5	−169.5	−67.1	170.2		
Ser28	−92.6	116.3	179.1	61.3			
Ser29	−147.8			59.7			

Table IV Hydrogen Bonds in IAPP^{H} (20–29) in Different Environments Obtained Using Molecular Dynamics Simulations

Environment	Donor	Acceptor	Distance	Angle
Dielectric 1	Ser20 Hγ	Ser29 CO	1.89	138.1
	Asn22 NH	Leu27 CO	1.96	174.8
	Asn22 Hδ	Ala25 CO	1.90	174.4
	Gly24 NH	Asn22 CO	2.41	134.5
	Ser29 NH	Leu27 CO	2.24	139.8
	Ser29 Hγ	Ser20 OH	1.69	177.7
Dielectric 2	Asn21 Hδ	Ser29 OH	2.33	139.5
	Ser28 Hγ	Ser20 CO	1.83	176.0
Dielectric 80	Asn22 NH	Leu27 CO	2.36	140.5
	Leu27 NH	Asn22 CO	2.40	143.1
	Ser29 Hγ	Ser20 CO	2.27	129.2

and Leu27 NH. These hydrogen bonds are not present in other environments. Apart from the hydrogen bonds discussed here, the minimum energy structures are also stabilized by hydrogen bonds that are formed between side chain groups; these data are also given in Table IV.

Intercarbon Distances

Since the analysis of various intercarbon distances is useful in predicting the secondary structure of a peptide, various intercarbon distances from the backbone of the minimum energy conformation of IAPP^{H}(20–29) peptide are measured and the data are given in Table V. All the intercarbon distances obtained from the MD simulations are in close agreement with the SSNMR experimental results reported in the literature.[10] The distance obtained for C′ of Gly24 and C_α of Ala25 in the MD was found to be 2.47 Å in the case of vacuum structure, and 2.48 Å in the case of model membrane and model aqueous solution environments. This observation is also in good agreement with the SSNMR experimental results of 2.43 Å.[10] The $C_i^\alpha - C_{i+3}^\alpha$ distances in the peptide, from residues Phe23 to Ile26, fall in the range 4.45–5.71 Å in all the environments. It should be mentioned here that the ^{13}C-^{13}C distances measured from the rotational resonance magic angle spinning, SSNMR, experiments on human amylin powder sample are of very high accuracy. There are low energy structures that emerge from the simulations, albeit not the lowest energy minimum structures, and that agree with the limited experimental data; thus, we have a model

Table V Comparison of Intercarbon Distances Measured (in Å Units) from the Minimum Energy Conformers of the IAPP^{H} (20–29) Peptide, Obtained Using Molecular Dynamics Simulations in Different Environments, and from the Reported Experimental Solid-State NMR Results[10]

	Dielectric 1		Dielectric 2		Dielectric 80		Ref. 10	
Residue	$C_{\alpha i}$, C'_{i+1}	C'_i, $C_{\alpha i+2}$	$C_{\alpha i}$, C'_{i+1}	C'_i, $C_{\alpha i+2}$	$C_{\alpha i}$, C'_{i+1}	C'_i, $C_{\alpha i+2}$	$C_{\alpha i}$, C'_{i+1}	C'_i, $C_{\alpha i+2}$
Ser20	4.9	6.1	4.7	4.8	4.6	5.0		
Asn21	4.5	4.9	4.7	5.0	4.7	5.6		
Asn22	4.7	4.9	5	6.2	4.8	5.7		
Phe23	4.9	5.5	4.4	5.1	4.6	4.9	4.6 ± 0.2	5.0 ± 0.2
Gly24	4.3	4.7	4.5	4.9	4.3	4.6	4.7 ± 0.2	
Ala25	4.7	4.8	4.7	5.0	4.7	5.1	4.8 ± 0.1	5.1 ± 0.2
Ile26	4.8	5.5	4.7	4.9	4.6	5.2		
Leu27	4.7	4.8	4.9	5.8	4.7	5.2		
Ser28	4.6		4.9		4.8			
Ser29								

Table VI

	900 K	600 K	450 K	375 K	340 K	320 K	300 k
Equilibration	20 ps	20 ps	10 ps	10 ps	5 ps	5 ps	5 ps
Dynamics	100 ps	40 ps	40 ps	40 ps	20 ps	20 ps	20 ps

for the entire peptide that is consistent with the experimental data and we hope it can provide a basis for additional experiments to confirm or disprove the model. In addition, the conformations reported in the present study will be valuable in the selection of ^{13}C nuclei pairs for further distance measurements using SSNMR experiments.

Simulated Annealing

Simulated annealing under different environments was carried out by heating the system [$IAPP^H(20–29)$] to 900 K and cooling it back to 300 K in seven phases. Structure obtained after the two-step energy minimization procedure was used as the starting structure for the simulated annealing studies. Phase 1 was the heating phase, which took the system to 900 K, and phase 2 to phase 7 were the cooling phases, which brought back the system to 300 K (900 ⇒ 600 ⇒ 450 ⇒ 375 ⇒ 340 ⇒ 320 ⇒ 300 K). Each dynamics phase consisted of the following steps:

1. Heat/Cool the system and equilibrate at a particular temperature for the desired time interval and carry out dynamics for the desired time according to Table VI.
2. Instantaneous configurations selected at 1 ps interval along the dynamics trajectories were minimized using the conjugate gradient method until the convergence criteria is achieved as discussed in the previous section.
3. Minimum energy conformation found along the trajectory of each phase was saved and used as the starting conformation for the next phase.

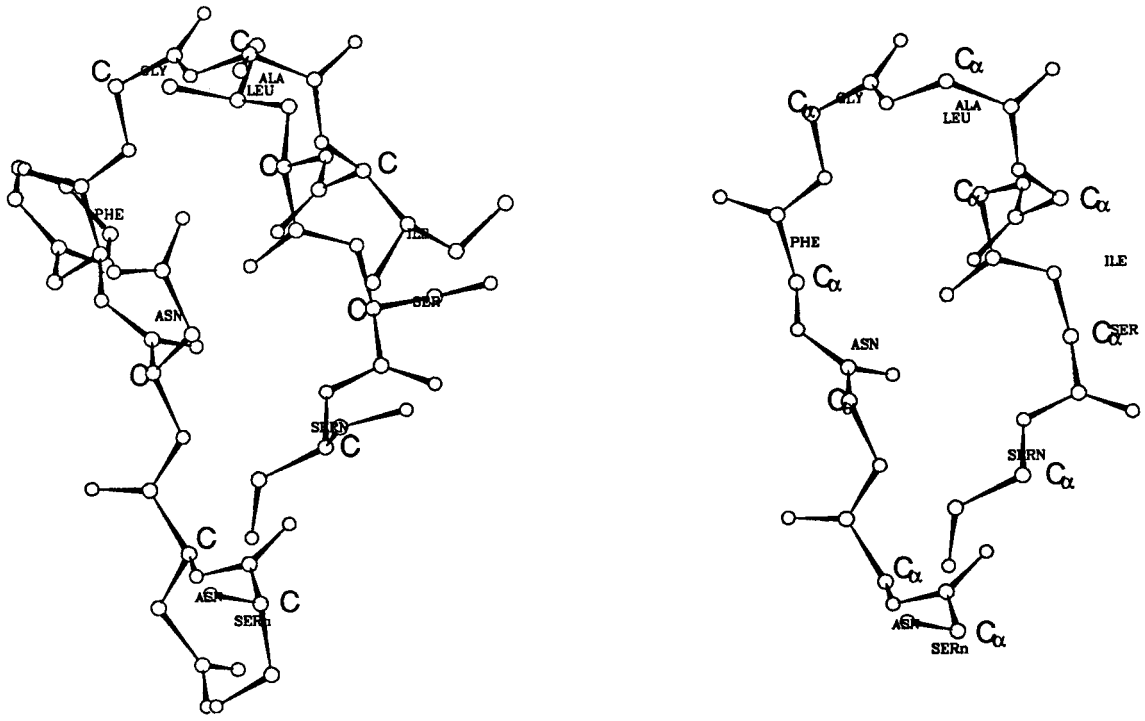

FIGURE 7 Minimum energy structure of $IAPP^H(20–29)$ in vacuum obtained from the simulated annealing procedure. Hydrogen atoms of the peptide are not shown. Backbone of the structure is shown on the right side.

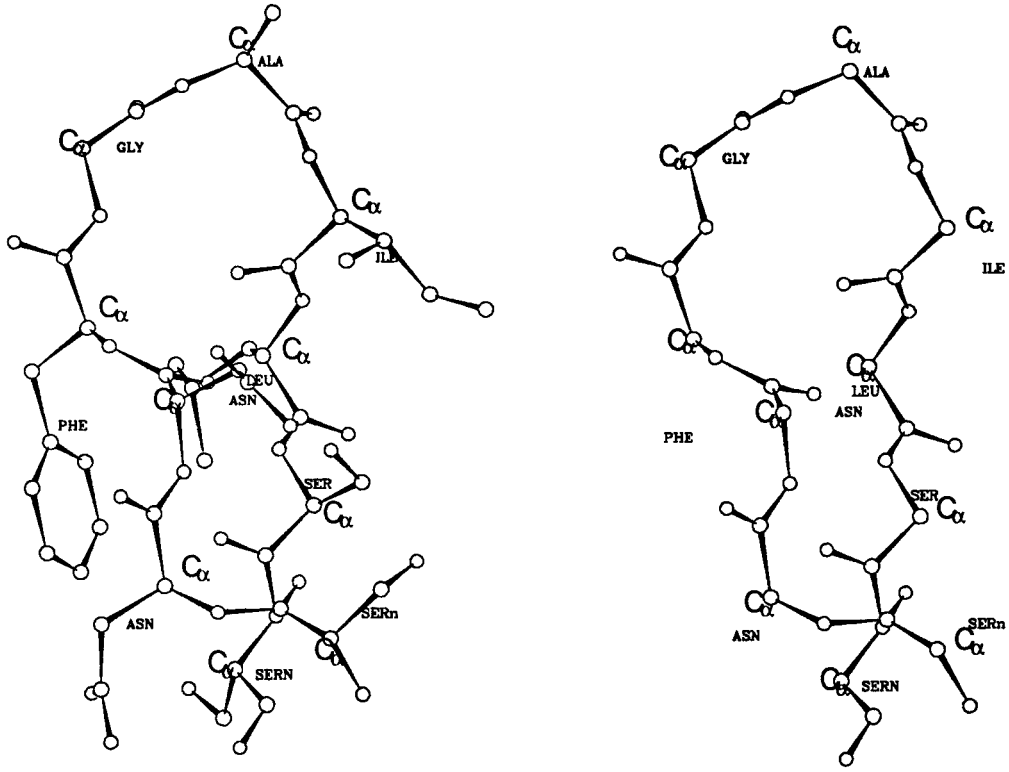

FIGURE 8 Minimum energy structure of IAPP^{H}(20–29) in the model membrane obtained from the simulated annealing procedure. All hydrogen atoms are omitted. Backbone of the structure is shown on the right side.

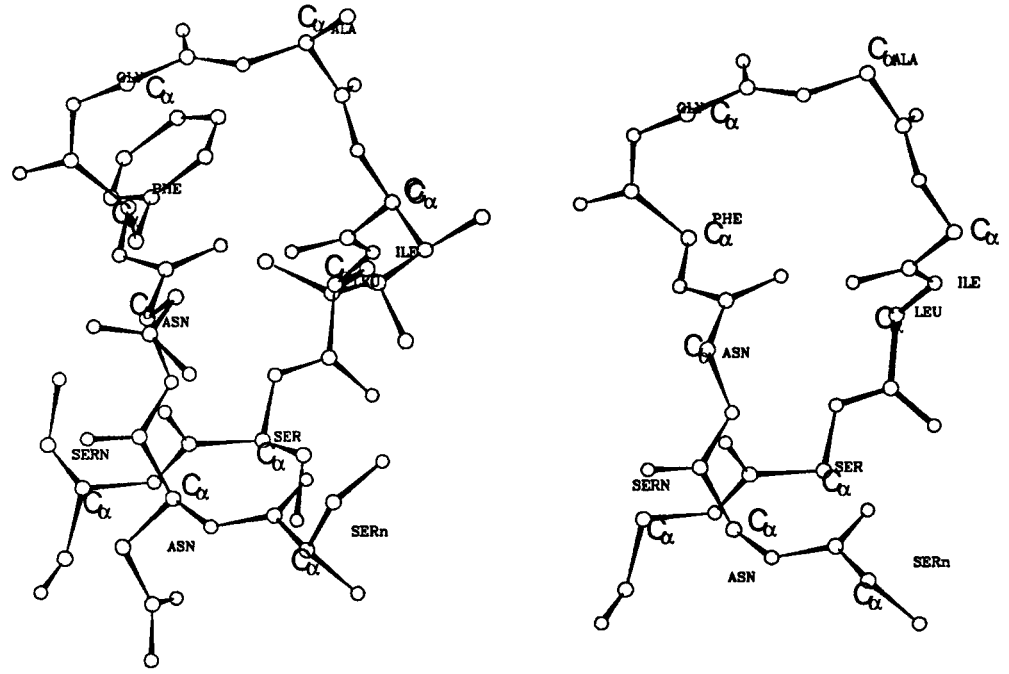

FIGURE 9 The minimum energy structure of IAPP^{H}(20–29) in model aqueous solution obtained from the simulated annealing procedure. Hydrogen atoms of the peptide are not shown. Backbone of the structure is shown on the right side.

Table VII Comparison of the Energy (kcal/mol) of the Conformers of IAPP^H (20–29) Obtained Through Molecular Dynamics and Simulated Annealing

	Molecular Dynamics	Simulated Annealing
Dielectric 1	78.69	74.23
Dielectric 2	101.71	89.61
Dielectric 80	100.41	93.00

Shown in Figures 7–9 are the minimum energy conformers obtained for IAPP^H(20–29) in different environments using the simulated annealing protocol. It is evident from Figures 7–9 that the acceptable conformers obtained from the simulated annealing studies, like those obtained from MD studies, also show a strong preference toward turn structures. Table VII compares the energy of the minimum energy conformers of IAPP^H(20–29) obtained from MD and simulated annealing studies. Simulated annealing consistently explored the low energy conformers in all the environments studied that are studied in the presented work.

Analyzing the dihedral angles of structures shown in Figures 7–9 revealed that, irrespective of the environment, the ϕ value of Gly24 was positive and that of other residues were negative. Various intercarbon distances were also measured from the conformers shown in Figures 7–9. Consistently, the distance measured between C_α Gly24 and C′ Ala25 and between C′ Ala25 and C_α Leu27 matched well with SSNMR results[10] under all environments, whereas other distances measured from the structures shown in Figures 7–9 show large deviation from those measured from the experimental results.[10]

Minimum energy conformers obtained through simulated annealing studies have lower energy when compared those obtained from MD studies. Intercarbon distances measured from the conformers obtained via simulated annealing are compared with the reported SSNMR experimental results in Table VIII. It is apparent that the calculated distances deviate from the experimentally predicted values. For example, the distance between C_α of Phe23 and C′ of Gly24 in model aqueous solution deviates by +1.1 Å from the SSNMR data.

CONCLUSIONS

Molecular dynamics simulations and simulated annealing studies were carried out to analyze the various conformational behavior of a peptide fragment, spanning 20–29 residues, of human amylin. In the absence of any useful solution-state nmr data on this peptide, a simple restraint-free MD was carried out in different environments, namely, vacuum, dielectric 2, and dielectric 80. In addition, simulated annealing studies were also carried out on IAPP^H(20–29) in all the three environments. From the detailed unrestrained MD studies, it can be safely concluded that IAPP^H(20–29) is folded to turn structures irrespective of the environments. The minimum energy conformers obtained in model aqueous solution and vacuum exhibited a similar

Table VIII Comparison of Intercarbon Distances Measured (in Å Units) from the Minimum Energy Conformers of the IAPP^H (20–29) Peptide, Obtained Via Simulated Annealing at Different Environments, and from the Reported Experimental Solid-State NMR Results[10]

	Dielectric 1		Dielectric 2		Dielectric 80		Ref. 10	
Residue	$C_{\alpha i}$, C'_{i+1}	C'_i, $C_{\alpha i+2}$	$C_{\alpha i}$, C'_{i+1}	C'_i, $C_{\alpha i+2}$	$C_{\alpha i}$, C'_{i+1}	C'_i, $C_{\alpha i+2}$	$C_{\alpha i}$, C'_{i+1}	C'_i, $C_{\alpha i+2}$
Ser20	4.81	4.86	4.63	4.90	4.64	4.93		
Asn21	4.71	5.60	4.76	5.57	4.81	5.61		
Asn22	4.72	5.34	4.87	5.61	4.76	4.03		
Phe23	5.00	5.77	4.92	5.72	3.50	5.53	4.6 ± 0.2	5.0 ± 0.2
Gly24	4.56	4.61	4.49	4.80	4.66	5.30	4.7 ± 0.2	
Ala25	4.38	5.10	4.48	5.39	4.60	5.21	4.8 ± 0.1	5.1 ± 0.2
Ile26	4.68	4.92	4.58	5.07	4.60	4.65		
Leu27	4.65	4.75	4.91	5.94	4.81	5.82		
Ser28	4.86		4.68		4.93			
Ser29								

structure. Even in the absence of any constraints on peptide bonds, *trans* conformation was preferred consistently by the peptide bonds. Turn structures were very well stabilized by the formation of hydrogen bonds between the backbone amide and carbonyl groups. Intercarbon distances obtained from the MD simulation studies agree very well with the reported experimental SSNMR measurements.

This work was supported by the start-up research funds from the Biophysics Research Division and Department of Chemistry. We thank Prof. E. Zuiderweg and the Biophysics Research Division for the computer time. The use of Insight II at the Department of Chemistry is gratefully acknowledged.

REFERENCES

1. Glenner, G. G., Eanes, M. D. E. D. & Wiley, G. A. (1988) *Biochem. Biophys. Res. Commun.* **155,** 608–614.
2. Westermark, P. & Wilander, E. (1978) *Diabetologia* **15,** 417–421.
3. Johnson, K. H., O'Brein, T. D., Jordan, K. & Westermark, P. (1989) *J. Am. Chem. Soc.* **135,** 245.
4. O'Brein, T. D., Hayden, D. W., Johnson, K. H. & Stevens, J. B. (1985) *Vet. Pathol.* **22,** 250.
5. Maloy, A. L., Longnecker, D. S. & Greenberg, E. R. (1981) *Human Pathol.* **12,** 917.
6. Westermark, P. & Grimerlius, L. (1972) *Upsala J. Med. Sci.* **77,** 91.
7. Lorenzo, A., Razzaboni, B., Weir, G. C. & Yankner, B. A. (1994) *Nature* **368,** 756–760.
8. Mirzabekov, T. A., Lin, M. C. & Kagan, B. L. (1996) *J. Biol. Chem.* **271,** 1988–1992.
9. Spencer, R. G. S., Halverson, K. J., Auger, M., McDermott, A., Griffin, R. G. & Lansbury, P. T. (1991) *Biochemistry* **30,** 10382–10387.
10. Griffiths, J. M., Ashburn, T. T., Auger, M., Costa, P. R., Griffin, R. G. & Lansbury, P. T., Jr. (1995) *J. Am. Chem. Soc.* **117,** 3539–3546.
11. Terzi, E., Holzemann, G. & Seelig, J. (1994) *Biochemistry* **33,** 1345–1350.
12. Nishi, M., Sanke, T., Nagamatsu, S., Bell, G. I. & Steiner, D. F. (1990) *J. Biol. Chem.* **265,** 4173–4176.
13. Terzi, E., Holzemann, G. & Seelig, J. (1994) *Biochemistry* **33,** 1345–1350.
14. Kowall, N. W., McKee, A. C., Yankner, B. A. & Beal, M. F. (1992) *Neurobiol. Aging* **13,** 537–542.
15. McLean, L. R. & Balasubramaniam, A. (1992) *Biochim. Biophys. Acta* **1122,** 317–320.
16. Cort, J., Liu, Z., Lee, G., Harris, S. M., Prickett, K. S., Gaeta, L. S. & Andersen, N. H. (1994) *Biochem. Biophys. Res. Commun.* **204,** 1088–1095.
17. Ashburn, T. T., Auger, M. & Lansbury, P. T. (1992) *J. Am. Chem. Soc.* **114,** 790–791.
18. Crippen, G. M. (1977) *J. Comput. Phys.* **26,** 449–452.
19. Havel, T. F., Kuntz, I. D. & Crippen, G. M. (1983) *Bull. Math. Biol.* **45,** 665–720.
20. Karplus, M. & McCammon, J. A. (1981) *CRC Crit. Rev. Biochem.* **9,** 293–349.
21. van Gunsteren, W. F., Kaptein, R. & Zuiderwig, E. R. P. (1983) in *Nucleic Acids Conformations and Dynamics*, Olson, W. K., Ed., CECAM, Orsay, pp. 79–92.
22. Hagler, A. T. (1985) in *The Peptides: Analysis, synthesis, Biology*, Vol. 7, Udenfriend, S., Meienhofer, J. & Hruby, V. J., Eds., Academic Press, Orlando, FL, pp. 213–299.
23. Hagler, A. T., Osguthorpe, D. J., Osguthorpe, P. D. & Hempel, J. C. (1985) *Science* **227,** 1309–1315.
24. Rizo, J., Koerber, S. C., Bienstock, R. J., Rivier, J., Hagler, A. T. & Gierasch, L. M. (1992) *J. Am. Chem. Soc.* **114,** 2852–2859.
25. Rizo, J., Koerber, S. C., Bienstock, R. J., Rivier, J., Gierasch, L. M. & Hagler, A. T. (1992) *J. Am. Chem. Soc.* **114,** 2860–2871.
26. Nigels, M., Clore, G. M. & Gronenborn, A. M. (1988) *FEBS Lett.* **239,** 129–136.
27. Braun, W. & Go, N. (1985) *J. Mol. Biol.* **186,** 611–626.
28. Sewell, J. C., Duve, H., Thorpe, A. & Altmann, J. A. (1995) *J. Biomol. Struct. Dynam.* **13,** 181–200.
29. Tobias, D. J., Klein, M. L. & Opella, S. J. (1993) *Biophys. J.* **64,** 670–675.
30. Wilmot, C. M. & Thornton, J. M. (1988) *J. Mol. Biol.* **203,** 221–232.